# REPORT DOCUMENTATION PAGE

*Form Approved*
*OMB No. 0704-0188*



| **1. REPORT DATE** *(DD-MM-YYYY)* | **2. REPORT TYPE** | **3. DATES COVERED** *(From - To)* |
|---|---|---|
| December 2013 | Technical Paper | December 2013- January 2014 |

**4. TITLE AND SUBTITLE**
Parametric Trends in the Combustion Stability Characteristics of a Single-Element Gas-Gas Rocket Engine

**5a. CONTRACT NUMBER**
In-House

**5b. GRANT NUMBER**

**5c. PROGRAM ELEMENT NUMBER**

**6. AUTHOR(S)**
Harvazinski, Sankaran, and Talley

**5d. PROJECT NUMBER**

**5e. TASK NUMBER**

**5f. WORK UNIT NUMBER**
Q0A1

**7. PERFORMING ORGANIZATION NAME(S) AND ADDRESS(ES)**

Air Force Research Laboratory (AFMC)
AFRL/RQRC
10 E. Saturn Blvd.
Edwards AFB CA 93524-7680

**8. PERFORMING ORGANIZATION REPORT NO.**

**9. SPONSORING / MONITORING AGENCY NAME(S) AND ADDRESS(ES)**
Air Force Research Laboratory (AFMC)
AFRL/RQR
5 Pollux Drive
Edwards AFB CA 93524-7048

**10. SPONSOR/MONITOR'S ACRONYM(S)**

**11. SPONSOR/MONITOR'S REPORT NUMBER(S)**
**AFRL-RQ-ED-TP-2013-267**

**12. DISTRIBUTION / AVAILABILITY STATEMENT**
Distribution A: Approved for Public Release; Distribution Unlimited. PA#13560

**13. SUPPLEMENTARY NOTES**
Conference paper for the 52nd AIAA Aerospace Sciences Meeting, National Harbor, Maryland, 13-17 January 2014.

**14. ABSTRACT**
Combustion instability continues to be a challenge in the design of rocket engines. The use of computational fluid dynamics (CFD) simulations screen potential designs offers the ability to reduce the number of costly tests and improve understanding of the underlying instability mechanism. In this study a series of axisymmetric CFD simulations are used to investigate the instability sensitivity to four design changes. The design changes are selected in an attempt to reduce the level of instability. The parameters considered are the combustor wall temperature, the effect of adding swirl to the fuel injector and two geometric changes, namely, fuel injector area reduction and the introduction of a chamfer in the injector face. The simulations show that both the wall temperature and swirl are able to significantly lower the amplitude by 70%. The results of the geometric changes are mixed with both decreases and increases in the instability amplitude. The parametric study has enhanced the understanding of the instability mechanisms by demonstrating that the when a continuous fuel supply to the combustor is maintained the instability amplitude is decreased.

**15. SUBJECT TERMS**

| **16. SECURITY CLASSIFICATION OF:** | | | **17. LIMITATION OF ABSTRACT** | **18. NUMBER OF PAGES** | **19a. NAME OF RESPONSIBLE PERSON** |
|---|---|---|---|---|---|
| | | | | | Doug Talley |
| **a. REPORT** | **b. ABSTRACT** | **c. THIS PAGE** | SAR | 23 | **19b. TELEPHONE NO** *(include area code)* |
| **Unclassified** | **Unclassified** | **Unclassified** | | | 661-525-6174 |

**Standard Form 298 (Rev. 8-98)**
**Prescribed by ANSI Std. 239.18**

# Parametric Trends in the Combustion Stability Characteristics of a Single-Element Gas-Gas Rocket Engine

Matthew E. Harvazinski*, Venkateswaran Sankaran†, and Douglas G. Talley‡
*Air Force Research Laboratory, Edwards AFB, CA, 93524*

**Combustion instability continues to be a challenge in the design of rocket engines. The use of computational fluid dynamics (CFD) simulations screen potential designs offers the ability to reduce the number of costly tests and improve understanding of the underlying instability mechanism. In this study a series of axisymmetric CFD simulations are used to investigate the instability sensitivity to four design changes. The design changes are selected in an attempt to reduce the level of instability. The parameters considered are the combustor wall temperature, the effect of adding swirl to the fuel injector and two geometric changes, namely, fuel injector area reduction and the introduction of a chamfer in the injector face. The simulations show that both the wall temperature and swirl are able to significantly lower the amplitude by 70%. The results of the geometric changes are mixed with both decreases and increases in the instability amplitude. The parametric study has enhanced the understanding of the instability mechanisms by demonstrating that the when a continuous fuel supply to the combustor is maintained the instability amplitude is decreased.**

## Nomenclature

| | |
|---|---|
| $A$ | Area |
| $\mathtt{AR}$ | Area reduction |
| $c$ | Sound speed |
| $f$ | Frequency |
| $H_r$ | Source term |
| $\ell$ | Length |
| $p$ | Pressure |
| $p'_{\mathrm{ptp}}$ | Peak-to-peak pressure fluctuation |
| $u_r$ | Radial velocity |
| $u_z$ | Axial velocity |
| $u_\theta$ | Azimuthal velocity |
| $\mathbf{u}$ | Velocity |
| $\varphi_s$ | Swirl angle |
| $\rho$ | Density |
| $\mathsf{Z}$ | Mixture fraction |

## I. Introduction

Combustion instabilities have plagued rocket engine development since the 1950's. For instance, the development of the F-1 engine required over 2000 full-scale tests during a three year period.[1] While the F-1 is an extreme example, it is by no means unique as documented by Blomshield in his historical review

*Scientist, AIAA Member.
†Senior Scientist, AIAA Member.
‡Research Physical Scientist, AIAA Associate Fellow.

of instabilities in production rocket engines.[2] One of the major challenges is the lack of suitable analytical models for combustion instability, which has resulted in the need for extensive testing and ad hoc post-design changes to correct for problems. Recently, the use of computational fluid dynamics (CFD) to simulate reacting flows has shown success in predicting combustion instability for a variety of configurations including both liquid rocket engines and gas turbines.[3–12] The high-fidelity simulation results furnish a vast array of information not available through traditional experimental diagnostics or reduced-order models, including three-dimensional unsteady flowfields, heat release, mixture fractions, and vorticity. The design engineer is therefore able to explore the underlying mechanisms contributing to instability and to make appropriate design changes to control the stability characteristics of the engine. Importantly, this entire process can take place during the design phase well before the engine is built. The present paper demonstrates such a process by exploring the sensitivity of design changes on the stability characteristics of an unstable single-element gas-centered shear-coaxial liquid rocket engine.

The chosen configuration is the continuously variable resonance chamber or CVRC. The CVRC has been designed to tune in stable and unstable combustor responses by varying the oxidizer post length.[13,14] For the present study, we select an unstable oxidizer post length and then make several design changes to the injector and the chamber to determine their effects on the stability response. In all cases, the post-length is maintained at 5.5 in and the combustion chamber length is 15 in. The fuel is methane and the oxidizer is decomposed hydrogen peroxide. The oxidizer flow is choked upstream of the post and the combustor has a choked nozzle at the downstream end, thereby isolating the acoustics in the post-combustor combination. Specific design changes include variation of the fuel port dimensions, the introduction of swirl in the fuel stream, the use of a chamfer in the combustor head-end and variation of the combustor wall temperature. In each case, the parameters are varied so as to try and stabilize the highly unstable baseline configuration.

Recent simulations have demonstrated the ability to successfully simulate both stable and unstable post lengths. Moreover, the computational results have provided insight into the underlying physics leading to the occurrence of combustion instabilities.[3] Two modes of unstable behavior have been observed. In both cases, the cycle starts with a cyclic interruption in the fuel supply due to the high pressure wave advancing upstream from the combustor into the injector assembly. Following this, the fuel flow resumes but it accumulates without burning for a period of time. In the first mode of instability, referred to as the post interaction mode, the returning pressure wave in the post promotes enhanced mixing of the fuel and oxidizer leading to strong combustion. In the second mode of instability, which is referred to as the vortex transport mode, the fuel is transported even further into the recirculation zone before it starts to burn. In both cases, the combustion causes a large pressure spike, which coincides with the pressure increase due to the returning pressure wave in the combustor that completes the cycle. The 5.5 in post-length case which is our baseline here is characterized by the former mechanism, i.e., the post interaction mode. We note that the latter vortex transport mechanism generally leads to larger pressure spikes because a greater amount of unburnt fuel has accumulated in the combustor.

Figure 1 gives a close-up view of the injector region for the baseline case, showing the disrupted incoming fuel (Fig. 1a) and the corresponding heat release upstream of the dump plane (Fig. 1 b). Figure 1c shows a plot of the dynamic pressure, $\frac{1}{2}\rho u^2$, and the unsteady pressure, $p - \bar{p}$, in the fuel injector. The timing of the plots in Figures 1a and 1b corresponds to the instance when the pressure at the head-end of the combustor is high, which occurs between 30.35 ms and 30.55 ms in Figure 1c. The fuel interruption is caused by two phenomena. First, there is increased mixing in the shear-layer due to vorticity generation via the baroclinic torque. This promotes combustion upstream of the combustor allowing fuel to be consumed before entering the combustor (see Figure 1b). Second, the large amplitude wave interacts with the annular fuel film pushing the fuel upstream away from the combustor (Figure 1a) and in some cases behind the injector. This aspect is also evident in Figure 1c during the period when the instantaneous pressure fluctuation is larger than the dynamic pressure head, indicating that the momentum flux is insufficient to drive the fuel into the combustor. The combination of the increased fuel consumption and the fuel redirection result in the fuel flow interruption event that is a key aspect of the instability cycle. In contrast, for stable configurations, the fuel supply is continuous and there is no observed burning upstream of the dump plane. In this paper, we examine various design changes targeted towards controlling these events and thereby controlling the stability characteristics. Specifically, many of the changes are targeted towards keeping the fuel film intact throughout the cycle in order stabilize the combustion response.

The outline of the paper is as follows. In the next section, we discuss the four design changes being pursued here: (1) area change of the fuel injector, (2) introduction of swirl in the fuel stream, (3) addition of

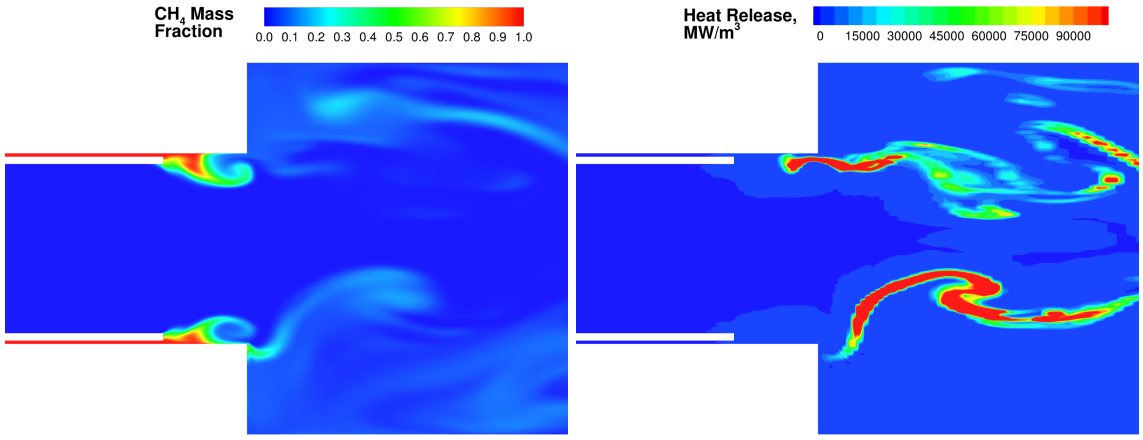


(a) Fuel mass fraction near the dump plane.

(b) Heat release near the dump plane.

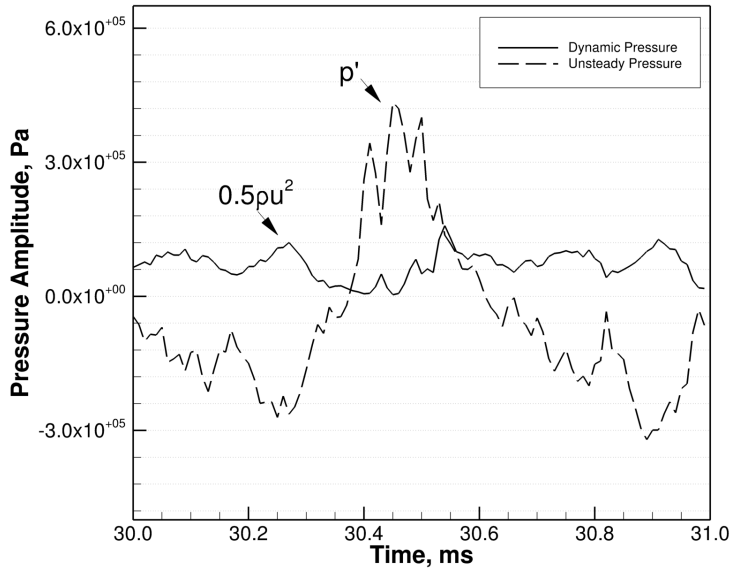


(c) Dynamic and unsteady pressure in the fuel injector for a single cycle of an unstable simulation.

Figure 1: Sources of instability, (a) and (b) show an instance in time where the incoming fuel flow is disrupted. Notice the heat release upstream of the dump plane and the fuel mass fraction void in the same region.

a chamfer at the injector face, and (4) variation in the combustor wall temperature. We then briefly describe the detached eddy simulation (DES) model used in these parametric studies. For simplicity, the simulations are restricted to axisymmetric flow which allows detailed parametrics to be done at a fraction of the cost of full 3D simulations. Our previous studies have confirmed that qualitative trends are well-predicted by axisymmetric simulations. The results section catalogs the effects of the design changes on the stability characteristics and provides a discussion of the associated physical phenomena to help explain the trends. We then conclude by offering some suggested directions for future research.

## II. Proposed Design Changes

This work is an attempt to look at the sensitivity of design changes on the observed instability characteristics for the unstable 5.5 in oxidizer post length. There are four changes of interest, lowering combustor wall temperature, switching to a swirling fuel injector, and two geometric changes. The first geometric change to the injector is the reduction of the fuel injector size and the second change is to add a chamfer to the injector in combination with a swirling fuel injector. We note that the overall objective is to utilize the sensitivity to better understand the instability phenomena and to demonstrate the utility of such high-fidelity simulations to investigate design changes.

### A. Fuel Injector Area Reduction

One option to overcome the momentum deficit would be to increase the fuel mass flow rate but this would decrease the oxidizer to fuel ($O/F$) ratio. In fact, pushing the operation from fuel lean to fuel rich has been shown to increase the observed levels of instability which is not desirable for this study.[15] Instead, the area of the fuel injector is reduced while holding the mass flow rate constant which gives the desired effect of a larger dynamic pressure without changing the $O/F$ ratio. Calculating the new injector size to overcome the fluctuating pressure is not a straightforward computation; reducing the area is likely to affect the stability of the system and thus the targeted pressure amplitude that must be overcome. A parametric study is used to capture the effect of injector area and the area reduction is defined as,

$$\texttt{AR} = 1 - \frac{A_r}{A_o} \tag{1}$$

where $A_r$ is the reduced area and $A_o = 0.045\,\text{in}^2$ is the original area. Table 1 shows the injector dimensions and corresponding areas for the baseline case and the three targeted area reductions. In all cases, the inner radius remains fixed and the outer radius is reduced. The height of the backstep is increased to match the reduction in injector height so that all other dimensions remain fixed.

Table 1: Geometric parameters for the fuel injector area reduction study.

| Parameter | AR | | | |
|---|---|---|---|---|
| | 0% | 20% | 40% | 60% |
| Injector area, $\text{in}^2$ | 0.045 | 0.036 | 0.027 | 0.018 |
| Inner Radius, in | 0.438 | 0.438 | 0.438 | 0.438 |
| Outer Radius, in | 0.454 | 0.451 | 0.448 | 0.445 |

### B. Wall Temperature

The baseline computations utilize an adiabatic wall boundary condition, which is incorrect because in the experiment there is heat loss through the metal chamber walls. No wall temperature or heat flux measurements are currently available from the experiment but a computational study by Garby et al. found that by imposing an outward heat flux the instability could be completely damped.[4] There is also experimental data showing that when the first third of the metal chamber is replaced with a quartz wall the transition point from unstable to stable combustion changes for the longer oxidizer post lengths. We note that the quartz wall mimics an adiabatic boundary condition and therefore the stability trends are qualitatively consistent

with the aforementioned computational observations.[3] In the present study, wall temperatures of 300 K, 600 K, 900 K, and 1200 K are evaluated.

### C. Swirl

Swirl stabilization has been used to mitigate instabilities in gas turbines, since the swirling fuel flow can produce a central toroidal recirculation zone which promotes flame stabilization.[16] For rocket applications swirl injectors are less sensitive to manufacturing defects and less susceptible to cavitation compared to jet type injectors. Swirl injectors have also been used to suppress high-frequency combustion instability.[17] A swirling fuel flow is typically added though geometric features which direct the fuel into the combustor at an angle relative to the core flow direction. This study is limited to two-dimensional axisymmetric simulations where the geometric features needed to add swirl cannot exist. It is however possible to solve an additional conservation equation for the axisymmetric circumferential momentum and supplement the existing radial momentum equation with a source term which accounts for the added swirling velocity. The additional source term in the radial momentum equation is,[18,19]

$$H_r = \frac{\rho u_\theta^2}{r} - \mu\left(\frac{2u_r}{r} - \frac{2}{3}\nabla\cdot\mathbf{u}\right) \tag{2}$$

and the axisymmetric circumferential momentum equation is,

$$\frac{\partial \rho u_\theta}{\partial t} + \frac{1}{r}\frac{\partial}{\partial r}\left(r\rho u_r u_\theta\right) + \frac{\partial}{\partial z}\left(\rho u_z u_\theta\right) = -\frac{\rho u_r u_\theta}{r} + \frac{1}{r^2}\frac{\partial}{\partial r}\left(r^3\mu\frac{\partial}{\partial r}\left(\frac{u_\theta}{r}\right)\right) + \frac{\partial}{\partial z}\left(\mu\frac{\partial u_\theta}{\partial z}\right) \tag{3}$$

In Equation 3 the variation of the viscosity in the viscous term is assumed to be constant with respect to the radial coordinate eliminating a $\frac{\partial \mu}{\partial r}$ term. Adding swirl to the flow generates a positive radial pressure gradient which is proportional to the swirl velocity,[16]

$$\frac{\partial p}{\partial r} \sim \rho\frac{u_\theta^2}{r} \tag{4}$$

This pressure gradient acts to keep the fuel film against the wall. The change in the radial pressure gradient also affects the baroclinic torque, which is the vector product of the density and pressure gradients. At the inlet the swirl is specified as an angle, $\varphi_s$, where the circumferential velocity is related to the incoming axial velocity though the equation,

$$u_\theta = u_z \cdot \sin\left(\varphi_s\right) \tag{5}$$

For the current study swirl angles of 3°, 6°, 9°, and 12° are considered.

### D. Chamfer

The use of a chamfer in addition to swirl allows the axial pressure wave to further push the fuel against the chamfered wall instead of upstream in the axial direction. The chamfer used for this study is shown in Figure 2, and has a length, $b$, of 3.81 mm which represents slightly more than a third of the total cup length, $L$, which is 10.16 mm. The angle of the chamfer is 45°.

## III. Simulation Details

Three-dimensional simulations remain expensive for large parametric investigations typically requiring an order of magnitude more computational resources for each simulation. For this reason, the strategy used for the parametric studies is to learn from two-dimensional simulations and make intelligent choices as to which limited three-dimensional cases should be undertaken. Fourteen simulations are performed to investigate the parameter space which addresses the sensitivity to the four possible stabilizing design changes presented in the previous section. The simulations are segregated into five groupings, baseline (BL), area reduction (AR), wall temperature (TW), swirl (S), and chamfer (C). The details of each case are summarized in Table 2. All other parameters remain fixed for each simulation including mass flow rates, inlet temperatures, and initial conditions.

The mesh is nearly identical for each case with only minor differences in the region surrounding the injector for the area reduction and chamfer cases were there are geometric changes. The mesh contains

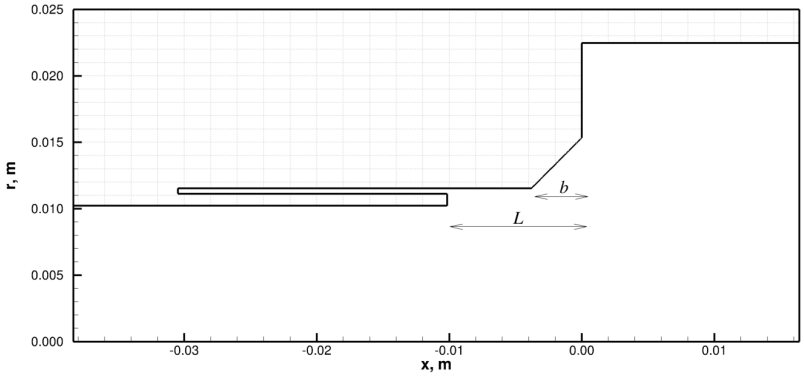


Figure 2: Geometric details of the chamfer used in the injector.

Table 2: Test matrix.

| Case | Combustor Wall Boundary Condition | Fuel Injector Area | Chamfered | Swirl |
|---|---|---|---|---|
| BL | Adiabatic | Standard | No | None |
| AR-1 | Adiabatic | 20% Reduction | No | None |
| AR-2 | Adiabatic | 40% Reduction | No | None |
| AR-3 | Adiabatic | 60% Reduction | No | None |
| TW-1 | $T = 300\,\mathrm{K}$ | Standard | No | None |
| TW-2 | $T = 600\,\mathrm{K}$ | Standard | No | None |
| TW-3 | $T = 900\,\mathrm{K}$ | Standard | No | None |
| TW-4 | $T = 1200\,\mathrm{K}$ | Standard | No | None |
| S-1 | Adiabatic | Standard | No | 3° |
| S-2 | Adiabatic | Standard | No | 6° |
| S-3 | Adiabatic | Standard | No | 9° |
| S-4 | Adiabatic | Standard | No | 12° |
| C-1 | Adiabatic | Standard | Yes | 6° |
| C-2 | Adiabatic | Standard | Yes | 12° |

approximately 315,000 grid points with fully resolved boundary layers, a requirement for the thermal wall boundary conditions. A single step global reaction is used to model the combustion,[20]

$$CH_4 + 2\,O_2 \longrightarrow 2\,H_2O + CO_2 \tag{6}$$

The use of a global reaction model allows for the coupling of pressure and reaction rate to be included without introducing a large number of species equations which must be solved in a coupled algorithm. Turbulence is accounted for using a hybrid LES/RANS model with k-$\omega$ serving as the underlying model.[21–23] Simulations are performed using the GEMS CFD code.[24–26] Previous two-dimensional simulations have been found to produce lower amplitudes than their three-dimensional counterparts and experiments but are still able to reproduce the stability trends and underlying physical phenomena.[5,6]

# IV. Results

All simulations were run time-accurately for 80 ms. This length of simulation provides a stationary time-averaged flowfield and sufficient cycles for analysis after a 30 ms initial transient. The observed peak-to-peak amplitude and frequency of the first mode are summarized in the next subsection giving an overview of the results. Following the summary, pertinent results for each of the four design changes are presented in the subsequent sections.

## A. Instability Amplitude

The instability amplitudes and frequencies of the first mode are shown in Table 3. The frequency and peak-to-peak pressure are found using a PSD analysis of the unsteady pressure signal. The pressure signal is located at the wall 14.5 in from the backstep, and the analysis is performed on the final 50 ms of data yielding a frequency resolution of 20 Hz. The peak-to-peak pressure is found by integrating under the PSD peak of the first mode.

For the area reduction study only AR-2 (40% reduction) is successful in reducing the instability amplitude, with the amplitude reduction being about 59.8%. The other two cases, AR-1 and AR-3, which had less and more area reduction respectively give roughly the same amplitude as the baseline case. The frequency increases slightly with decreasing injector size but remains close to the baseline case.

The wall temperature has a noticeable effect on the instability amplitude. Cases TW-1 and TW-2, which have the lowest wall temperatures, completely suppress combustion. The remaining two cases both show large reductions in the instability amplitude. The amplitude is reduced by 79.8% and 70.4% for cases TW-3 and TW-4 respectively. Interestingly, the frequency differs significantly from the baseline frequency which indicates that it is no longer the pure first longitudinal mode in the combustor that is being excited.

Peak-to-peak pressure amplitudes are also reduced by swapping the shear-coax injector for a swirl injector. Case S-3 (9°) provides the largest reduction in amplitude, 69.9%. Case S-1 with the least amount of swirl has the smallest reduction of 41.7%. The frequencies for all cases are slightly increased above the baseline value.

The addition of chamfer to the swirling fuel injector also reduces the instability amplitude. With 6° of swirl the instability is reduced by 11.5% while 12° of swirl provides a reduction in the amplitude of 57.6%. Compared to the swirling non-chamfered geometry, the chamfer provids some additional damping for the 12° case but amplifies the instability of the 6° case. The frequency of both chamfered cases is identical to their non-chamfered swirling counterparts.

This brief summary of the results suggests that the design changes are successful in reducing the amplitude, but an excited instability is still present in each case where combustion takes place. The results are demonstrative of a key challenge in understanding combustion instability and in the design of rocket engines, namely that small design changes can have large effects on the instability amplitude and frequency.

## B. Area Reduction

The objective of reducing the fuel injector area is to increase the dynamic pressure such that the magnitude of the dynamic pressure is always greater than the amplitude of the fluctuating pressure. Doing so should ensure that there is a steady supply of fuel into the combustor. Table 4 summarizes the relevant flow conditions. As expected the reduction in area generates an increase in the magnitude of the dynamic pressure. Despite

Table 3: Peak-to-peak pressure amplitude and frequency for the first mode.

| Case | $p'_{\text{ptp}}$, kPa | Frequency, Hz |
|---|---|---|
| Experiment | 387.15 | 1324 |
| BL | 135.19 | 1460 |
| AR-1 | 139.67 | 1440 |
| AR-2 | 54.28 | 1460 |
| AR-3 | 139.39 | 1520 |
| TW-1 | No observed combustion | |
| TW-2 | No observed combustion | |
| TW-3 | 27.34 | 1100 |
| TW-4 | 40.04 | 1020 |
| S-1 | 78.82 | 1480 |
| S-2 | 65.00 | 1480 |
| S-3 | 40.72 | 1480 |
| S-4 | 60.61 | 1480 |
| C-1 | 119.70 | 1480 |
| C-2 | 57.33 | 1480 |

the fact that each successive reduction has a higher dynamic pressure, the results in Table 3 suggest that there is an optimal injector size (velocity) because only AR-2 demonstrates lower peak-to-peak pressure amplitude. The change in the injector size also alters the mean chamber pressure where an increase of 160 kPa is observed between the baseline case and AR-3. The increase in mean pressure appears to be the result of the higher injection velocity which allows for better mixing and more complete combustion. The change in the mean pressure is also responsible for the increase in the instability frequencies observed in the AR series of simulations. It is possible that the higher mean pressure is also an artifact of the axisymmetric simulations which allow small amounts unburnt fuel to become trapped along the centerline as a result of the artificial boundary condition.

Table 4: Time-averaged conditions.

| Case | $\rho$, kg/m$^3$ | $u$, m/s | $\frac{1}{2}\rho u^2$, kPa | Increase in Dynamic Pressure | Mean Chamber Pressure, kPa | $p'_{\text{ptp}}$, kPa |
|---|---|---|---|---|---|---|
| BL | 8.92 | 114.81 | 587.89 | — | 1440. | 135.19 |
| AR-1 | 9.28 | 142.70 | 944.86 | 1.61 | 1496. | 139.67 |
| AR-2 | 9.53 | 187.29 | 1671.44 | 2.84 | 1513. | 54.28 |
| AR-3 | 10.41 | 254.57 | 3373.15 | 5.74 | 1601. | 139.39 |

A plot of the dynamic pressure and unsteady pressure is shown in Figure 3 for the baseline and three area reduction cases. Notice that despite the increase in dynamic pressure there are times when the unsteady pressure fluctuation remains larger than the dynamic pressure for each case. AR-2, which has the lowest peak-to-peak amplitude shows the lowest occurrence of this event. An important observation is that with the increasing fuel velocity there are larger unsteady variations of the dynamic pressure. This suggests that the instability is possibly the result of an injector velocity coupled phenomena. In fact, this additional unsteadiness of the dynamic pressure could be the reason that this method is not successful in consistently lowering the amplitude of the instabilities.

To quantify the effect that the injection velocity has on the mixing, the mixture fraction can be used to

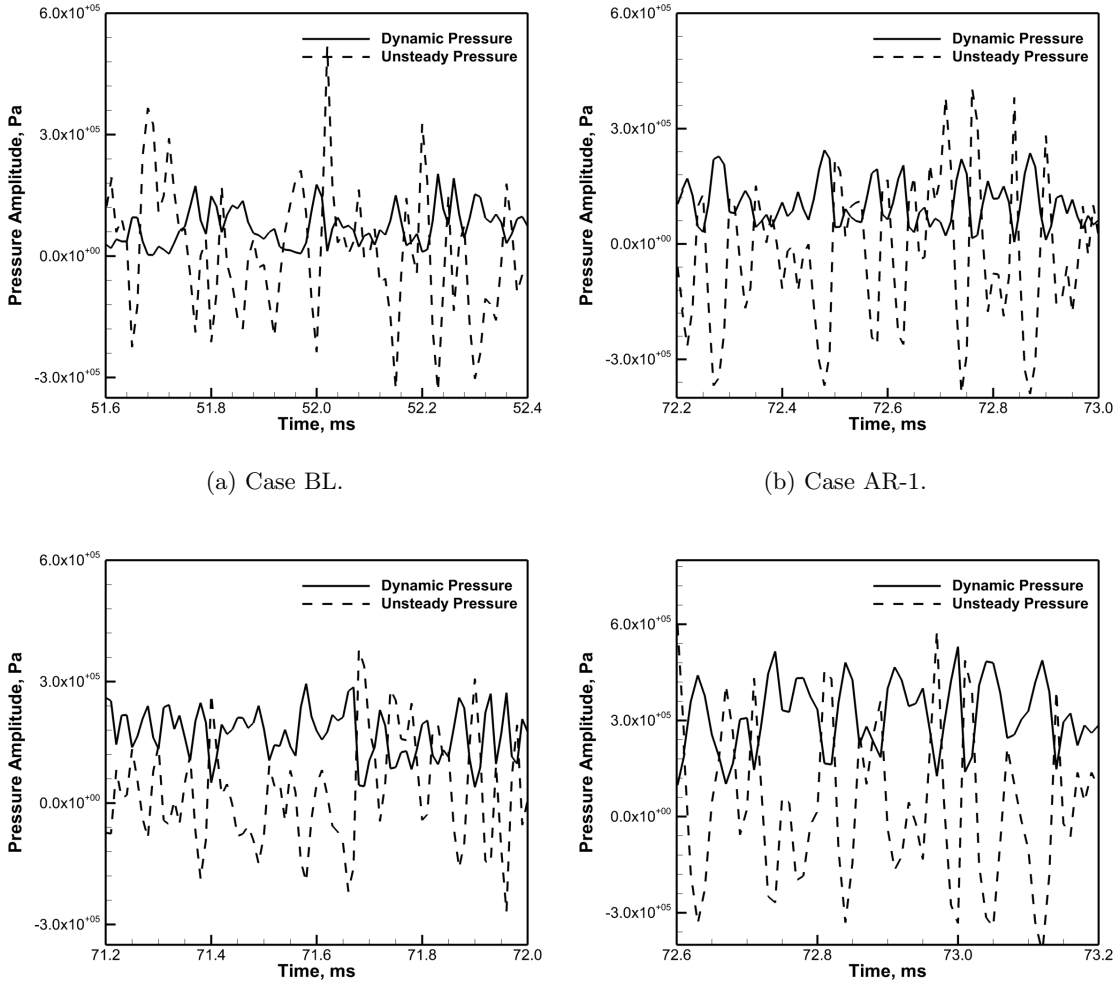


(a) Case BL.

(b) Case AR-1.

(c) Case AR-2.

(d) Case AR-3.

Figure 3: Dynamic pressure ($\frac{1}{2}\rho u^2$) and the unsteady pressure ($p - \overline{p}$) at the fuel injector.

visualize the mixedness of the flowfield. Define the mixture fraction, Z, to be,

$$\mathsf{Z} = \frac{\nu_{\text{st}} Y_{\text{CH}_4} - Y_{\text{O}_2} + Y^0_{\text{O}_2}}{\nu_{\text{st}} Y^0_{\text{CH}_4} + Y^0_{\text{O}_2}} \tag{7}$$

such that a value of unity is a region with pure fuel and a region of pure oxidizer has a value of zero. For the present operating condition, $\nu_{\text{st}} = 4.0$, $Y^0_{\text{CH}_4} = 1.0$ and $Y^0_{\text{O}_2} = 0.4235$. The time-averaged mixture fraction is shown in Figure 4. The lowest amplitude case, AR-2, shows the least amount of fuel present in the recirculation region. Recall that, for the baseline case, the combustion is governed by the so-called post-interaction mechanism which leads to the combustion taking place in the shear layer itself. The fact that the results for cases AR-1 and AR-3 show the fuel going into the recirculation region suggests that the mechanism has switched to the vortex transport mechanism where the combustion occurs further downstream and the resulting pressure spike is stronger. This explains why the instability amplitudes remain high for these two cases despite the higher fuel injection velocity. On the other hand, case AR-2 shows a greater similarity with the baseline case, which explains the agreement with the anticipated behavior, i.e., that the increase in fuel velocity reduces the amplitude of the instability. Nevertheless, we note that there is no definite trend and further computational studies are necessary to understand the behavior.

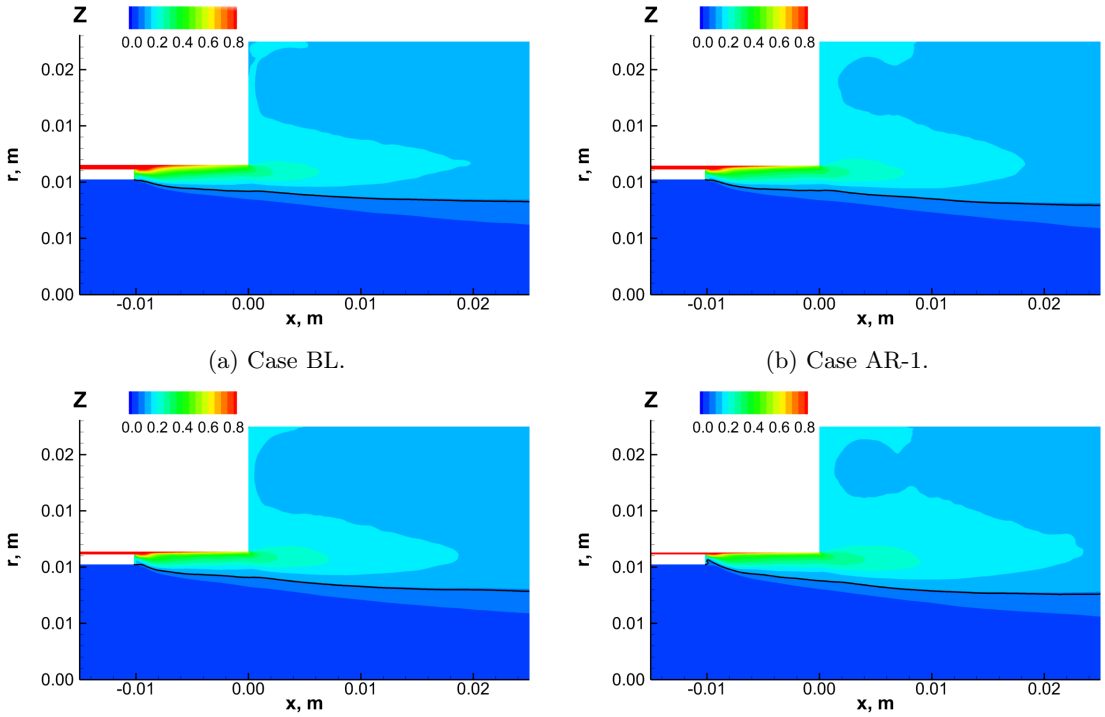


(a) Case BL.

(b) Case AR-1.

(c) Case AR-2.

(d) Case AR-3.

Figure 4: Mixture fraction near the fuel injector and backstep for the baseline case and three reduced area cases. Black line represents the stoichiometric mixture fraction ($\mathsf{Z}_{\text{st}} = 0.095739$).

### C. Combustor Wall Temperature

The baseline case utilizes an adiabatic wall temperature which prevents the loss of heat from the recirculation region through the walls. By imposing a uniform "cool" wall temperature, i.e., one that is lower than the wall temperature in the adiabatic limit, there can be heat loss through the walls, which should result in lower levels of combustion instability. Figure 5 shows the time- averaged temperature in the combustion region for each wall temperature case. The effect of wall temperature is apparent in the series of plots. For the two lowest wall temperatures, there is no combustion at all since the cooler wall temperatures prevent ignition from taking place. We note that introducing an igniter into the flow would have caused combustion

to initiate although we are not sure whether the resulting combustion would have been sustained. Increasing the wall temperature to 900 K is found to be sufficient for sustained combustion to take place. The effect of the imposed thermal boundary condition is readily apparent in the left inside corner of the combustor where the flow is noticeable cooler when compared to the adiabatic baseline case. We observe that the wall temperature in the baseline case is around 2600 K (showing some variation with axial position), which is significantly higher than any of the constant wall temperature cases shown here. We further note that the two cases TW-3 and TW-4 yield significantly lower levels of pressure fluctuation as shown in Table 3 and the frequency of the most unstable mode is observed to be significantly lower as well. Further discussions in this section are restricted to these two cases.

A quantitative comparison of the temperatures can be made by looking at the temperature as a function of axial position at specified radial positions. Figure 6 shows the average temperature and sound speed at two radial positions, $r = \frac{1}{3}R$ and $r = \frac{2}{3}R$. Looking first at the $r = \frac{1}{3}R$ position, the temperature for all three cases are initially similar until approximately 0.03 m from the backstep where the temperature in the adiabatic wall case begins to increases more rapidly through the combustion region. The specified wall temperature cases do not increase as rapidly and remain similar until 0.07 m from the backstep. When the chamber temperature reaches a steady value the final combustor temperature shows a variation of 240 K between TW-3 and BL. For the profiles farther away from the centerline, at a radial position $r = \frac{2}{3}R$, the profiles are dissimilar for the entire length of the combustor. Close to the backstep in the corner recirculation region there is a large temperature difference, approximately 250 K between the two fixed wall temperatures and the adiabatic wall. By 0.04 m downstream the two fixed wall temperature cases diverge and remain different for the remainder of the combustor. The specified wall boundary condition not only lowers the overall combustor temperature but lowers the temperature of recirculation gases and reduces the rate at which the temperature increases through the combustion region.

It is apparent that the heat loss through the walls leads to a weakening of the combustion instability. Moreover, the lower combustor temperatures would lead to reduced sound speeds and, consequently lower modal frequencies. The plot of sound speed (Figure 6) shows that the variation of the sound speed is similar for the baseline and wall temperature cases. The frequency of the first mode can be estimated using the definition of first longitudinal mode for pure acoustics,

$$f_{1\mathrm{L}} = \frac{c}{2\ell}. \tag{8}$$

Table 5: Estimated and measured frequencies.

| Case | Frequency, Hz | |
|---|---|---|
| | Measured | Estimated |
| BL | 1460 | 1405 |
| TW-3 | 1110 | 1330 |
| TW-4 | 1020 | 1355 |

Table 5 shows the measured frequency and the estimated frequency from Eq. 8 using the sound speed at the 0.25 m location. The predicted frequency of the baseline case is very similar to the observed frequency while the frequencies for TW-3 and TW-4 differ by over 200 Hz. This indicates that the wall temperature has done more than just change the chamber sound speed; in fact, it may also have changed the excited mode or mode shape. The observed frequencies of around 1100 Hz suggest that it is no longer a pure first longitudinal mode in the combustor that is being excited, but possibly some form of a combined post-combustor mode.

The mode shapes for cases BL and TW-4 are constructed using a dynamic mode decomposition (DMD) of the data.[27,28] The DMD uses 3000 snapshots spaced 0.01 ms apart. A one-dimensional representation of the pressure mode shape for the first excited mode is shown in Figure 7. The mode shape for TW-4 has the general shape of a 1L mode and and is similar to the baseline in the downstream end of the combustor away from the combustion. In the region of combustion, $0\,\mathrm{m} \leq x \leq 0.1\,\mathrm{m}$, there is a difference in the relative amplitude and shape which propagates into the oxidizer tube. For the lower wall temperature the pressure fluctuation at the backstep is larger, by a factor of 1.5, than the downstream fluctuation unlike the baseline case which has similar amplitudes near the backstep and the downstream location. It is possible that this

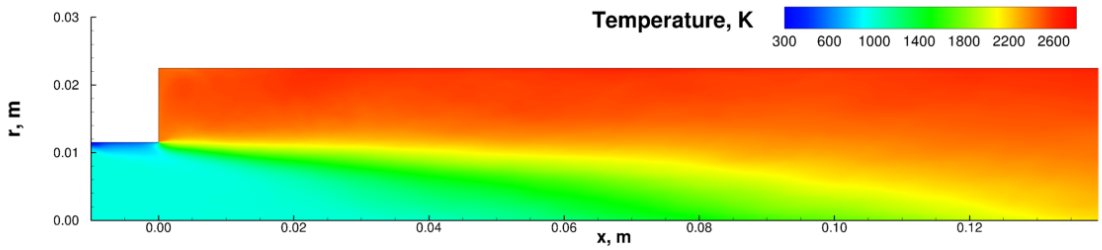


(a) Case BL.

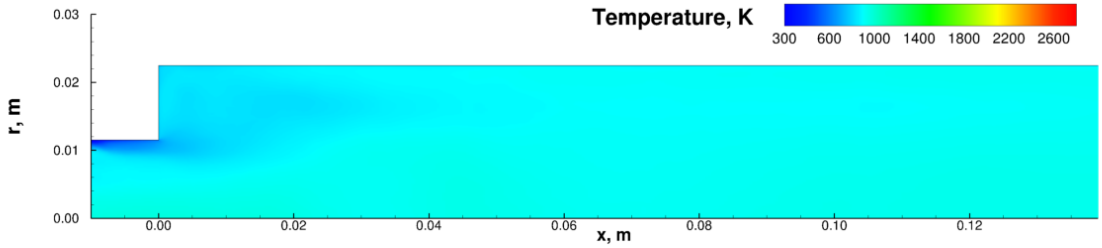


(b) Case TW-1.

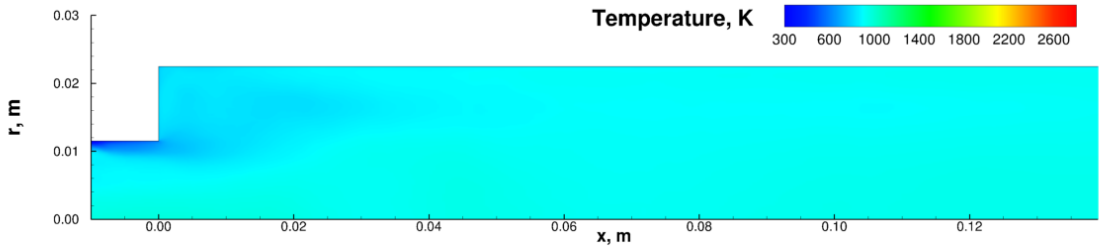


(c) Case TW-2.

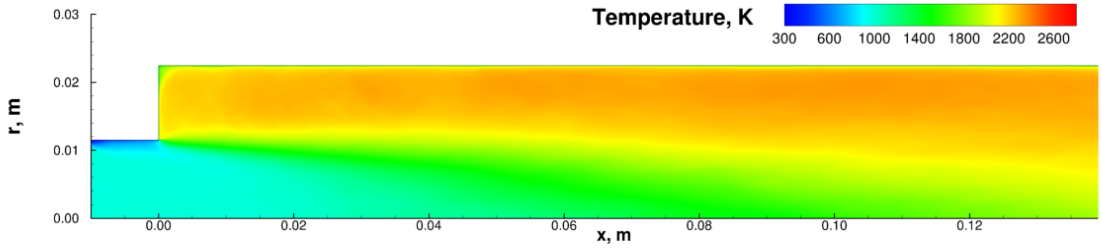


(d) Case TW-3.

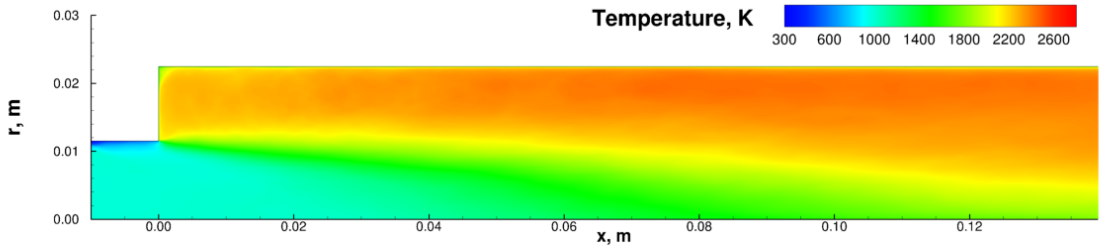


(e) Case TW-4.

Figure 5: Time averaged temperature in the combustor for the specified wall temperature cases. For TW-1 and TW-2 the temperature remains low throughout the entire combustor not just the region shown.

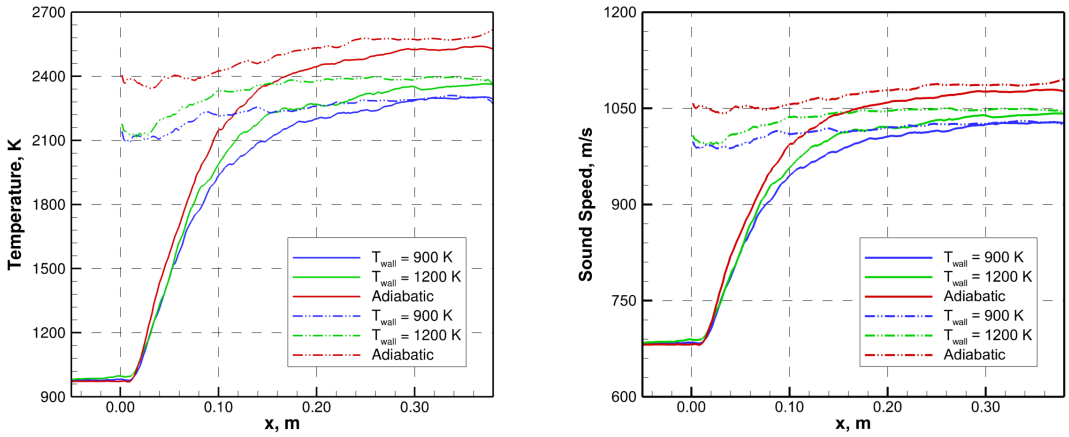


(a) Temperature.

(b) Sound Speed.

Figure 6: Time averaged temperature and sound speed in the combustor. Solid lines represent a radial position of $r = \frac{1}{3}R$ and dashed lines are for a radial position of $r = \frac{2}{3}R$. Cases TW-1 and TW-2 are not shown because of the absence of combustion.

mismatch in the amplitudes at the upstream and downstream locations detunes the resonance mode in the combustor and results in the lower frequency. Further analyses are necessary to confirm these trends.

Both the mode shape and temperature plots have shown substantial differences in the area where combustion takes place. A plot of the time-averaged combustion heat release and recirculation regions are shown in Figure 8. The heat release for the specified wall temperature cases are farther away from the centerline and combustor wall than the baseline case, but extends farther downstream. TW-3, which was the most stable case, shows no heat release upstream of the backstep while both BL and TW-4 show heat release upstream of the backstep, a feature which appears to increase the instability level. In summary, the specified wall temperature cases produce heat release patterns that are narrow, sitting just below the shear layer and extending farther downstream compared to the case with the adiabatic boundary condition. The corner recirculation regions are also observed to be more compact for TW-3 and TW-4 showing less radial breadth.

### D. Swirl

We next consider the effects of swirl in the fuel stream by replacing the shear-coax injector with a swirl-coax injector. As noted earlier, the pressure amplitude is reduced as a consequence of the swirling fuel flow. When the swirling fuel is injected, it mixes with the bulk oxidizer flow (which is not swirling) and, as a result, the swirl velocity quickly decays in the region away from the injector. However, it remains significant close to the injector walls. Figure 9 shows the swirl velocity component near the injector, while outside of this region the magnitudes are negligible. Larger swirl angles naturally lead to larger swirl velocities, with the swirl velocity ranging from 5.4 m/s (case S-1) to 21.2 m/s (case S-4), while the axial injection velocity is fixed at 103.8 m/s for all four cases. In all swirl cases, the swirl is confined to the wall region upstream of the backstep; in cases S-3 and S-4, the higher swirl velocities cause a swirl component to persist into the combustor, although by about 0.01 m downstream they are very small indicating that the fuel flow is well-mixed with the (non-swirling) oxidizer flow.

The swirl induced radial pressure gradient is shown for case S-4 in Figure 10 where it is compared with the baseline case. Both show strong gradients at the backstep corner. The negative pressure gradient, which will move fuel towards the centerline, is significantly reduced for the swirl cases compared to the baseline case. The swirling flow also has a thin layer of positive pressure gradient (red contour) along the wall which is absent in the baseline case. Both of these contribute to stabilization of the combustion because they help maintain a continuous supply of fuel into the combustor.

The continuous supply of fuel in the swirl cases, in turn, leads to an anchoring of the flame. This can be best visualized by looking at the unsteady heat release contours. A series of plots of the unsteady heat

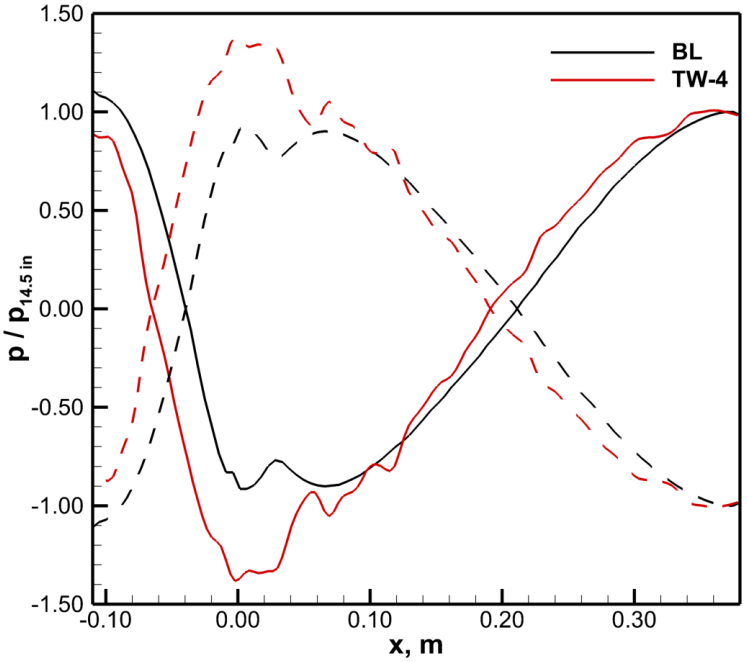


Figure 7: Pressure mode shape for the first excited mode.

release in the vicinity of the backstep for cases BL and S-3 is shown in Figure 11. For the three snapshots shown, which are representative of the overall behavior, the flame in the baseline case shows significant unsteadiness—there is initial heat release upstream of the backstep, the flame then gets detached and, eventually, it has moved away from the corner. We noted earlier that this was due to the disruption in the fuel flow in the unstable baseline case. In contrast, the swirling flow maintains a continuous supply of fuel and stabilizes flame by anchoring it to the corner of the back-step. Unsteady behavior is still observed in the three time-frames shown; but, the flame-anchoring clearly contributes to the reduced amplitudes of the pressure oscillations.

### E. Chamfer

The final study shows the added effect of including a chamfer in the injector face configuration. As shown earlier, the addition of the chamfer actually increases the combustion instability amplitude for lower swirl velocities, while it decreases it nominally for higher swirl velocities. Figure 12 shows three representative snapshots in time of the fuel concentration for the baseline and chamfered cases. The baseline case shows a disruption of the fuel flow in frames (a) and (c). The disruption is more severe in frame (c) where a substantial gap in the fuel is forming just upstream of the backstep. Contrast this behavior with the chamfered geometry where there is a continuous supply of fuel into the combustor. Notice that frame (g) shows an disruption of fuel near the injection point but a fuel rich annulus is present all the way from the injector to the chamfer corner. In frame (i) the pressure wave disrupts the fuel flow by pushing it into the chamfered region instead of upstream. For case C-1 frames (d-f) there is more unsteadiness with larger amounts of fuel entering the combustion region outside the hear layer.

Based on the $CH_4$ mass fraction it is expected that the chamfer alters the flowfield and the heat release distribution. The time-averaged heat release and streamlines are shown in Figure 13. The addition of the chamfer allows significant heat release to take place before the backstep at $x = 0$ in the chamfered volume. The primary recirculation region for the chamfered geometry starts at the upstream chamfer corner compared to the backstep corner of the original geometry. The more noticeable change is in the shape of the secondary recirculation region in the corner which has been compressed in the radial direction. The chamfer

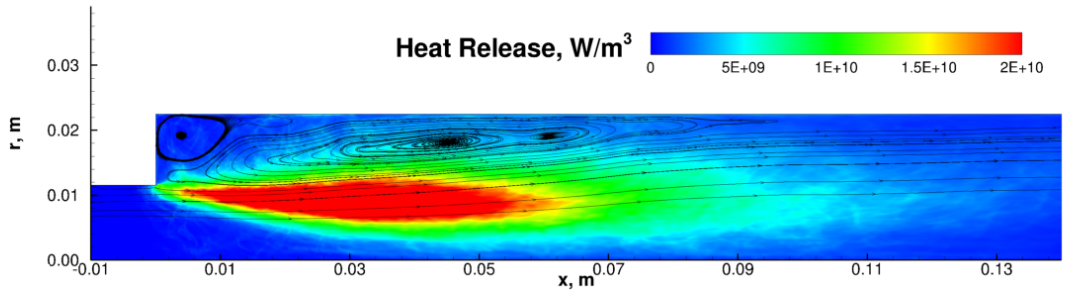


(a) Case BL.

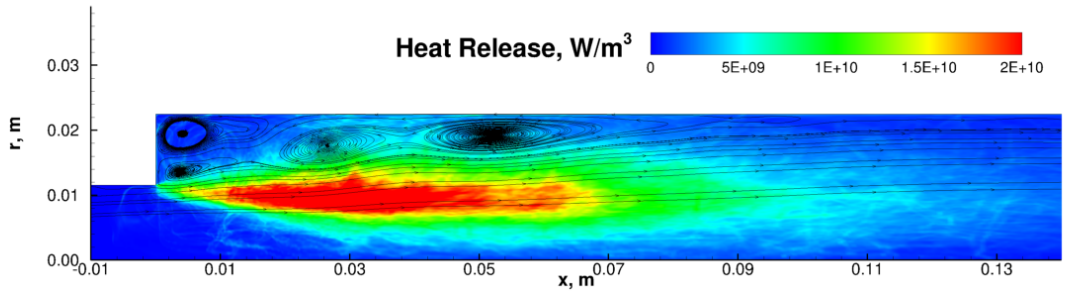


(b) Case TW-3.

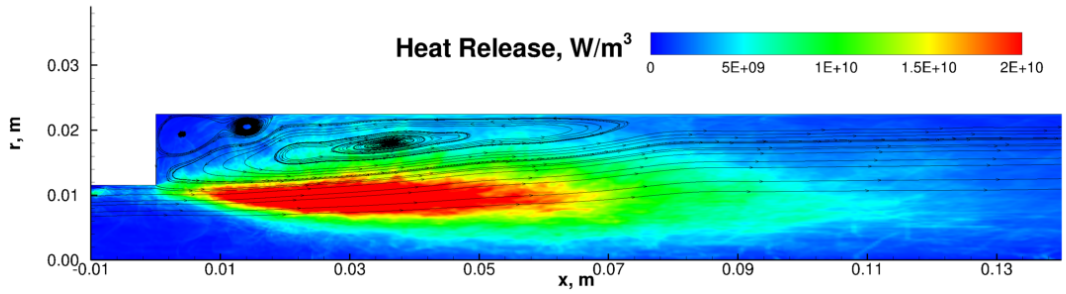


(c) Case TW-4.

Figure 8: Time averaged heat release and streamlines in the combustion region.

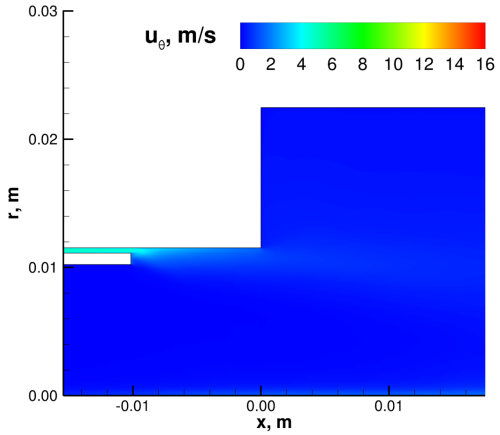


(a) Case S-1.

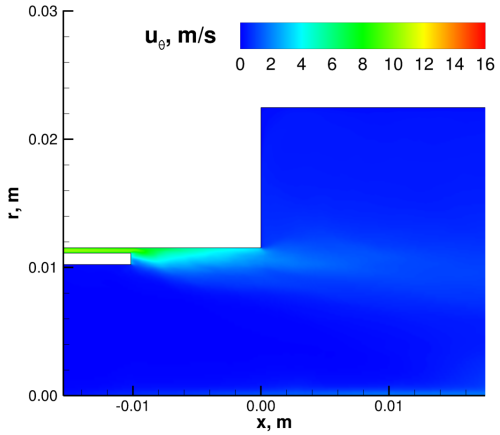


(b) Case S-2.

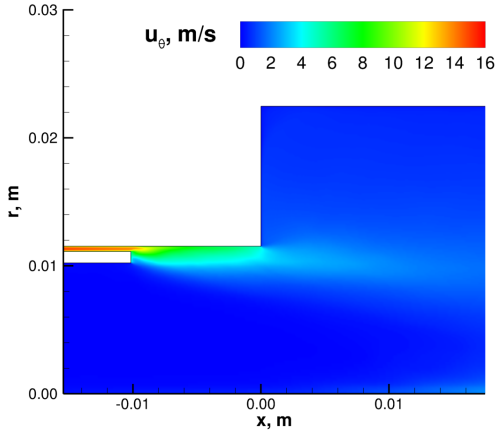


(c) Case S-3.

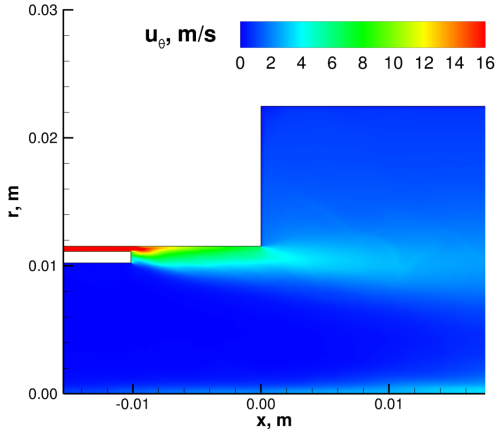


(d) Case S-4.

Figure 9: Swirl velocity near the injector.

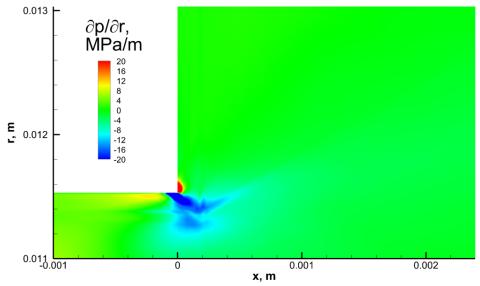


(a) Case BL.

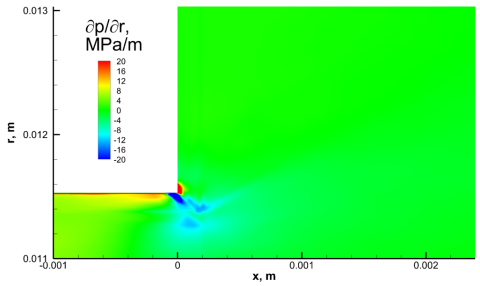


(b) Case S-4.

Figure 10: Radial pressure gradient near the backstep.

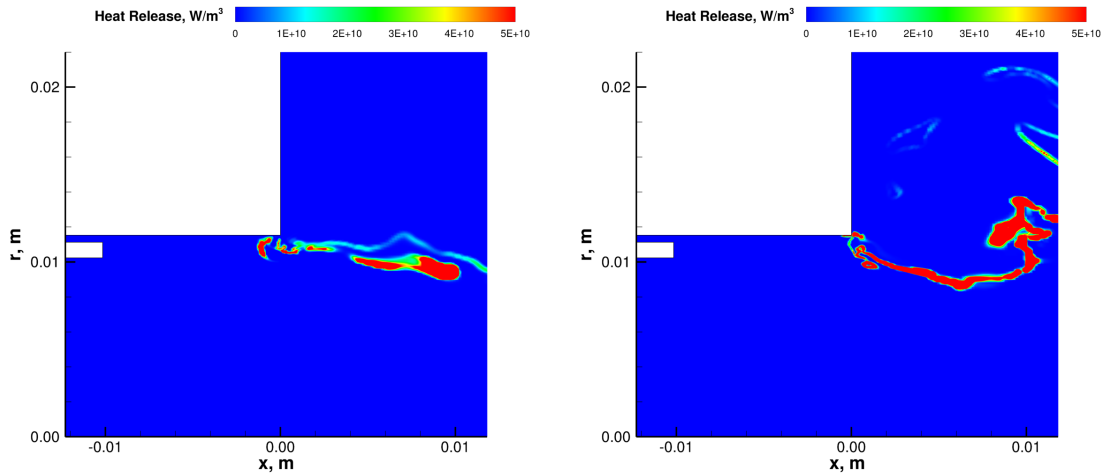


(a) Case BL.




(b) Case S-3.

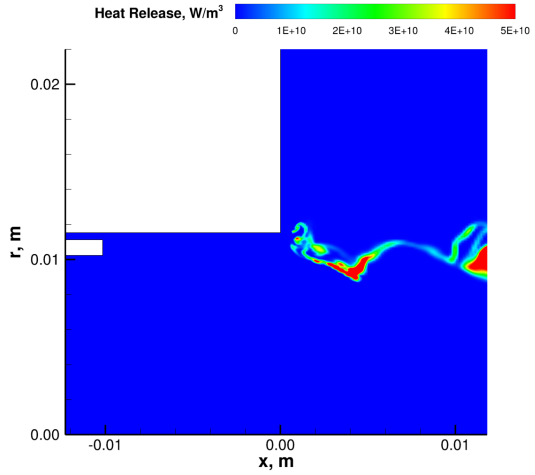


(c) Case BL.

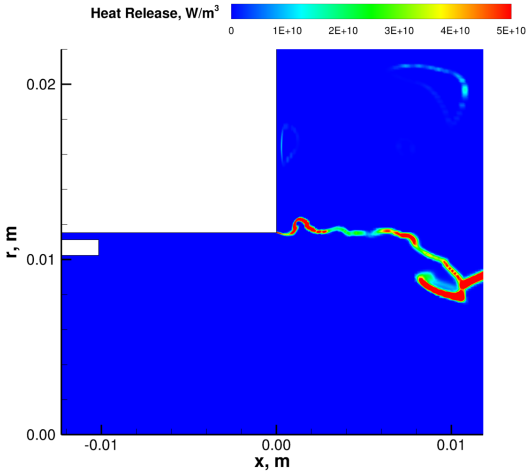


(d) Case S-3.

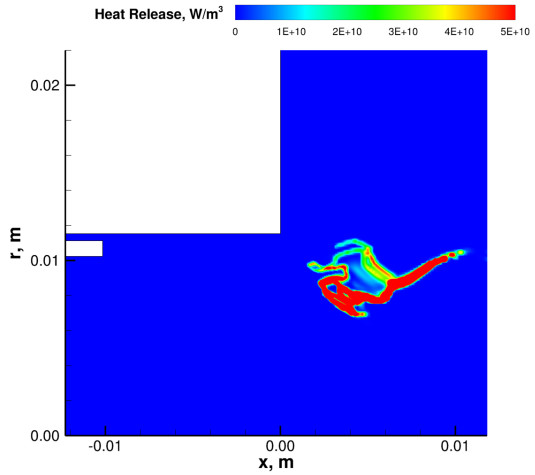


(e) Case BL.

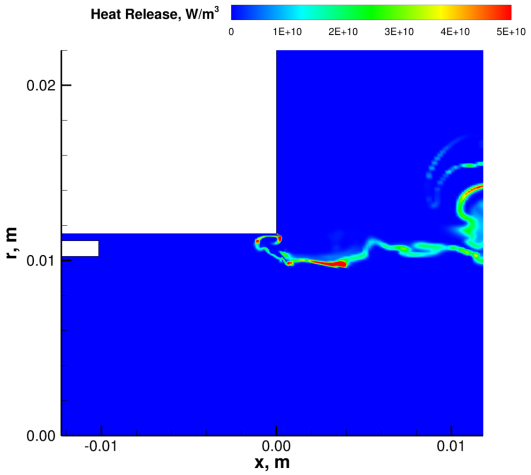


(f) Case S-3.

Figure 11: Unsteady heat release near the backstep. Notice how the heat release is attached near the backstep corner for the swirl case but is unattached for the baseline case.

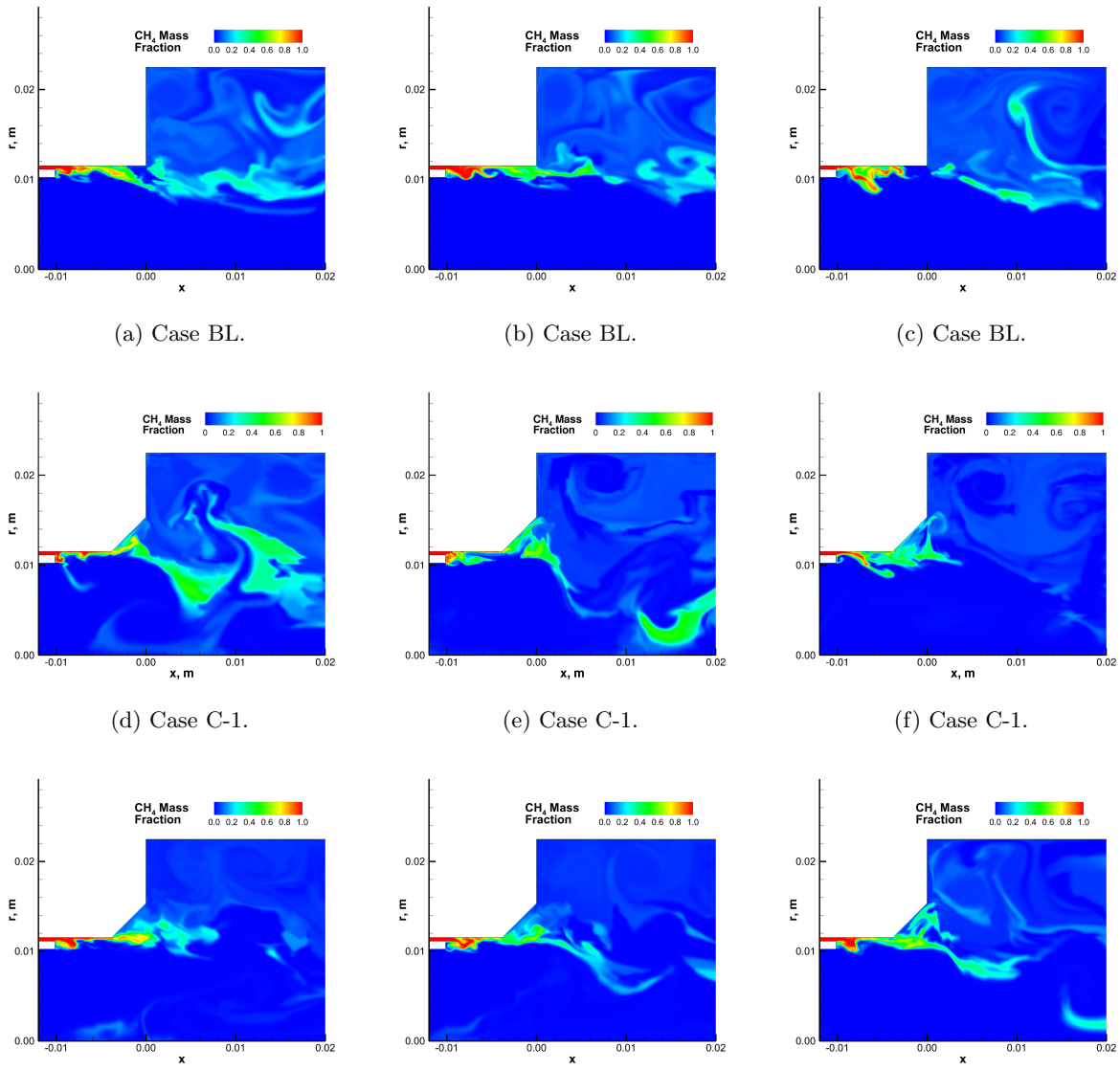


(a) Case BL. (b) Case BL. (c) Case BL.

(d) Case C-1. (e) Case C-1. (f) Case C-1.

(g) Case C-2. (h) Case C-2. (i) Case C-2.

Figure 12: Unsteady $CH_4$ concentrations near the backstep and chamfer.

and swirl distribute the heat release in the combustor over a wider volume. In the baseline case the elevated heat release (red contour) is 0.07 m from the centerline, adding a chamfer and swirl reduces that distance to 0.05 m. However, the time-averaged heat release and mixture fraction distributions do not identify why case C-2 is more stable than C-1.

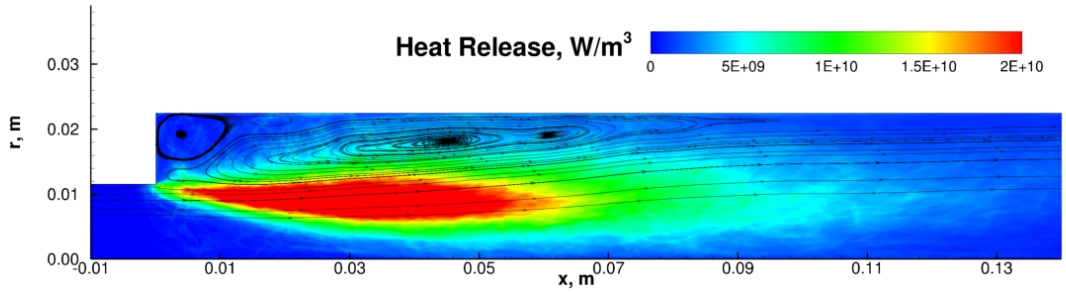


(a) Case BL.

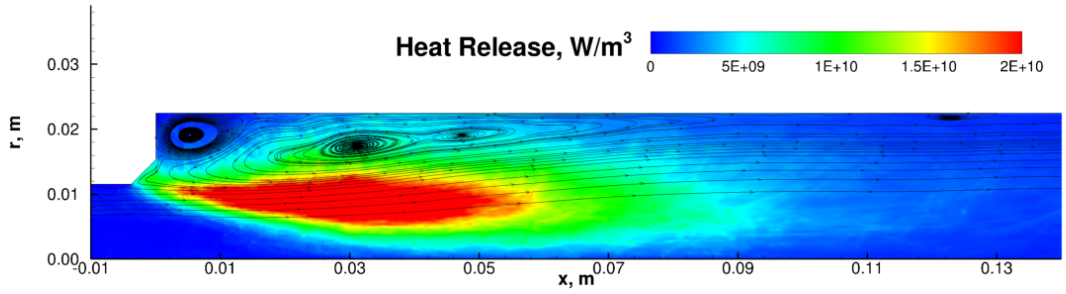


(b) Case C-1.

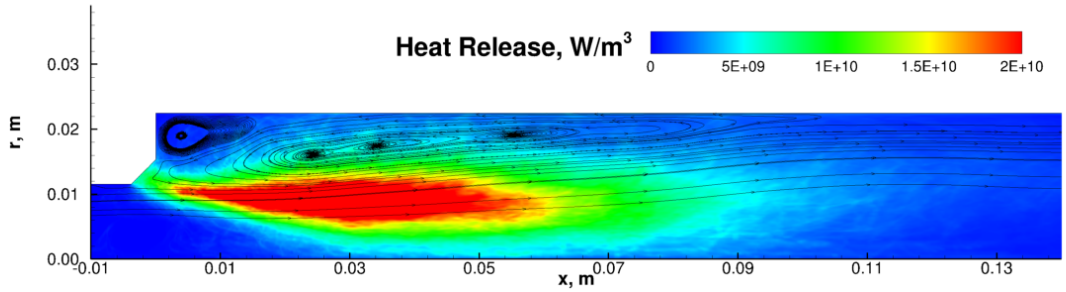


(c) Case C-2.

Figure 13: Time averaged heat release and streamlines in the combustion region for the chamfered cases.

It is necessary to consider the unsteady heat release profiles as shown in Figure 14. For case C-1, which is more unstable, the flame shows significant oscillations along chamfered surface while case C-2 shows a flame that is anchored near the upstream chamfer corner. The anchored flame, which was also observed in the swirl cases without the chamfer, is a stabilizing effect and is evidence that there is a regular supply of fuel into the combustor. Figure 14 shows snapshots of heat release for the two chamfered cases which demonstrates this unsteadiness. Additional parametrics of the chamfered geometry are necessary to establish these trends more definitely.

## V. Conclusions

Four design changes have been undertaken to control the combustion stability characteristics of an unstable singe-element gas-gas rocket combustor. In all, fourteen axisymmetric simulations were undertaken

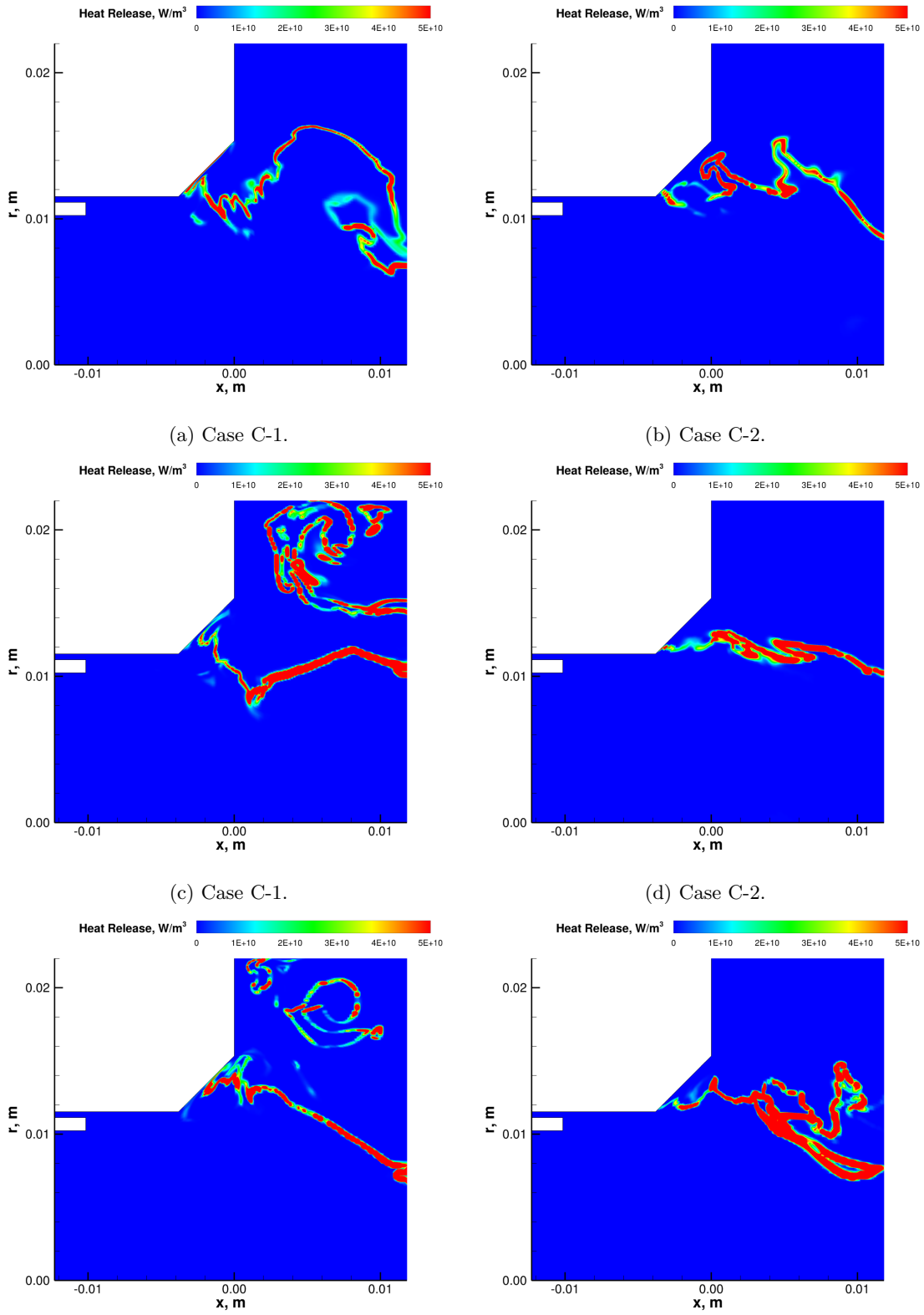


(a) Case C-1.

(b) Case C-2.

(c) Case C-1.

(d) Case C-2.

(e) Case C-1.

(f) Case C-2.

Figure 14: Unsteady heat release near the chamfered. Notice how the heat release oscillates along the length of the chamfer for case C-1 but remains anchored near the lower corner for case C-2.

to parametrically study these design changes, that included increasing the fuel velocity, introducing swirl in the fuel flow, adding a chamfer to the injector face configuration and systematically reducing the combustor wall temperature (i.e., by cooling the walls). Although no case showed fully stable combustion nearly all of the design changes showed lower instability amplitudes compared to the baseline case. The most successful methods of lowering the pressure amplitudes were reducing the combustor wall temperature and adding fuel swirl. Specifically reducing the wall temperature to 900 K (from its adiabatic value of 2600 K) as well as adding a swirl angle of 9-degrees were both shown to reduce the amplitude by 70%. The effect of wall temperature is evidently due to the energy lost to the combustor walls, which lowers the combustion response that is coupled with the combustor acoustics. The change in wall temperature also changes the observed most unstable frequency, which appears to be related to a subtle mode coupling between the injector post and the combustion chamber.

The swirling flow showed that the key mechanism for stabilizing the flame is due to the maintenance of a continuous flow of fuel in the injector, which causes the unsteady flame to remain anchored to the backstep throughout the cycle. In contrast, the baseline shear-coaxial injector shows that the fuel flow gets disrupted by the high amplitude pressure waves in the chamber, which in turn, cause the flame to alternately attach and detach. The addition of the chamfer to the swirl-flow cases shows that, at low swirl velocities, the chamfer can cause more flame unsteadiness, while, at higher swirl velocities, the chamfer seems to promote flame stabilization. The least successful design change was the reduction of the fuel injector area, which increases the dynamic pressure in order to counter the disruptive effect of the high amplitude pressure oscillations. However, the resulting increase in the fuel velocity appears to increase the degree of flame unsteadiness. Moreover, for some designs, the flowfield seems to cause the appearance of a vortex transport mode of instability wherein the uncombusted fuel is transported into the warm recirculation region before burning, resulting in relatively larger pressure spikes. Further studies of this velocity coupling effect are warranted before drawing definitive conclusions about the design. In summary, these studies showcase the usefulness of physics-based simulations to evaluate design changes that can influence the stability characteristics of rocket injectors and combustors. Future work will focus on extending a selected subset of these cases to full three-dimensional simulations, which will provide a more quantitative evaluation of these proposed designs.

## Acknowledgments

Computing resources were provided by the DoD High Performance Computing Modernization Program.

## References

[1]Oefelein, J. and Yang, V., "Comprehensive Review of Liquid-Propellant Combustion Instabilities in F-1 Engines," *Journal of Propulsion and Power*, Vol. 9, No. 5, September-October 1993, pp. 657–677.

[2]Blomshield, F., "Historical Perspective of Combustion Instability in Motors: Case Studies," *37th AIAA/ASME/SAE/ASEE Joint Propulsion Conference and Exhibit*, Salt Lake City, Utah, July 2001.

[3]Harvazinski, M., Huang, C., Sankaran, V., Feldman, T., Anderson, W., Merkle, C., and Talley, D., "Instability Mechanism in a Pressure-coupled Gas-gas coaxial rocket injector," *49th AIAA/ASME/SAE/ASEE Joint Propulsion Conference and Exhibit*, AIAA, San Jose, CA, July 2013.

[4]Garby, R., Selle, L., and Poinsot, T., "Analysis of the impact of heat losses on an unstable model rocket-engine combustor using large-eddy simulation," AIAA, Atlanta, GA, July 2012, AIAA Paper 2012-4085.

[5]Garby, R., Selle, L., and Poinsot, T., "Large-Eddy Simulation of Combustion Instabilities in a Variable-length Combustor," *Comptes Rendus Mécanique*, Vol. 341, No. 1-2, 2013, pp. 220–229.

[6]Harvazinski, M., Anderson, W., and Merkle, C., "Analysis of Self-Excited Combustion Instability using Two- and Three-Dimensional Simulations," *Journal of Propulsion and Power*, Vol. 29, No. 2, 2013, pp. 396–409.

[7]Angelberger, C., Veynante, D., and Egolfopoulos, F., "LES of Chemical and Acoustic Forcing of a Premixed Dump Combustor," *Flow, Turbulence and Combustion*, Vol. 65, 2000, pp. 205–222.

[8]Schmitt, P., Poinsot, T., Schuermans, B., and Geigle, K., "Large-eddy simulation and experimental study of heat transfer, nitric acid and combustion instability in a swirled high-pressure burner," *Journal of Fluid Mechanics*, Vol. 570, 2007, pp. 17–46.

[9]Huang, Y., Sung, H., Hsieh, S., and Yang, V., "Large-Eddy Simulation of Combustion Dynamics of Lean-Premixed Swirl-Stabilized Combustor," *Journal of Propulsion and Power*, Vol. 19, No. 5, September-October 2003, pp. 782–794.

[10]Wolf, P., Gicquel, L., Staffelbach, G., and Poinsot, T., "Grid Effects on LES Thermo-Acoustic Limit-Cycle of a Full Annular Aeronautical Engine," *Quality and Reliability of Large-Eddy Simulations II*, Vol. 16 of *ERCOFTAC Series*, Springer Netherlands, 2011, pp. 231–240.

[11]Kaufmann, A., Nicoud, F., and Poinsot, T., "Flow Forcing Techniques for Numerical Simulation of Combustion Instability," *Combustion and Flame*, Vol. 131, No. 4, December 2002, pp. 371–385.

[12]Martin, C., Benoit, L., Sommerer, Y., Nicoud, F., and Poinsot, T., "Large-Eddy Simulation and Acoustic Analysis of a Swirled Staged Turbulent Combustor," *AIAA Journal*, Vol. 44, No. 4, April 2006, pp. 741–750.

[13]Yu, Y., Sisco, J., Rosen, S., Madhav, A., and Anderson, W., "Spontaneous Longitudinal Combustion Instability in a Continuously-Variable Resonance Combustor," *Journal of Propulsion and Power*, Vol. 28, No. 5, 2012, pp. 876–887.

[14]Feldman, T., Harvazinski, M., Merkle, C., and Anderson, W., "Comparison Between Simulation and Measurement of Self-Excited Combustion Instability," *48th AIAA/ASME/SAE/ASEE Joint Propulsion Conference and Exhibit*, AIAA, Atlanta, GA, July 2012.

[15]Harvazinski, M., *Modeling Self-Excited Combustion Instabilities Using a Combination of Two- and Three-Dimensional Simulations*, Dissertation, Purdue University, West Lafayette, May 2012.

[16]Huang, Y. and Yang, V., "Dynamics and stability of lean-premixed swirl-stabilized combustion," *Progress in Energy and Combustion Science*, Vol. 35, 2009, pp. 293–364.

[17]Bazarov, V., Yang, V., and Puri, P., "Design and Dynamics of Jet and Swirl Injectors," *Liquid Rocket Thrust Chambers: Aspects of Modeling, Analysis, and Design*, edited by V. Yang, M. Habiballah, J. Hulka, and M. Popp, AIAA, Reston, VA, 2004, pp. 19–103.

[18]Tannehill, J., Anderson, D., and Pletcher, R., *Computational Fluid Mechanics and Heat Transfer*, Taylor and Francis, Philadelphia, PA, 2nd ed., 1997.

[19]Panton, R., *Incompressible Flow*, John Wiley & Sons, Hoboken, NJ, 3rd ed., 2005.

[20]Westbrook, C. and Dryer, F., "Simplified Reaction Mechanisms for the Oxidation of Hydrocarbon Fuels in Flames," *Combustion Science and Technology*, Vol. 27, 1981, pp. 31–43.

[21]Wilcox, D., "Formulation of the $k$-$\omega$ turbulence model revisited," *45th AIAA Aerospace Sciences Meeting and Exhibit*, AIAA, Reno, NV, January 2007.

[22]Spalart, P., Jou, W., Strelets, M., and Allmaras, S., "Comments on the feasibility of LES for wings on a hybrid RANS-LES approach," *1st U.S. Air Force Office of Scientific Research Office Conference on DNS/LES*, Columbus, OH, August 1997, pp. 137–148.

[23]Travin, A., Shur, M., and Splart, P., "Physical and numerical upgrades in the detached-eddy simulation of complex turbulent flows," *412 EUROMECH Colloquium on LES of Complex Transitional and Turbulence Flows*, Munich, October 2000.

[24]Li, D., Sankaran, V., Merkle, C., and Lindau, J., "A Unified Computational Formulation for Multi-Component and Multi-Phase Flows," *43rd AIAA Aerospace Sciences Meeting and Exhibit*, January 2005, AIAA Paper 2005-1391.

[25]Lian, C., Xia, G., and Merkle, C., "Solution-Limited Time Stepping to Enhance Reliability in CFD Applications," *Journal of Computational Physics*, Vol. 228, 2009, pp. 4836–4857.

[26]Li, D., Xia, G., Sankaran, V., and Merkle, C., "Computational Framework for Complex Fluids Applications," *3rd International Conference on Computational Fluid Dynamics*, Toronto, Canada, July 2004.

[27]Schmid, P., Li, L., Juniper, M., and Pust, O., "Applications of the Dynamic Mode Decomposition," *Theoretical Computational Fluid Dynamics*, Vol. 25, No. 1-4, 2011, pp. 249–259.

[28]Huang, C., Harvazinski, M., Anderson, W., and Sankaran, V., "Analysis of Self-Excited Combustion Instability using Decomposition Techniques," *51st AIAA Aerospace Science Meeting Including the New Horizons Forum and Aerospace Exposition*, January 2013.